Journal of Transactions in Systems Engineering
https://ijitis.org/index.php/JTSE
ISSN: 2806-2973
Volume 2, Issue 1
DOI: https://doi.org/10.15157/JTSE.2024.2.1.156-169
Received: 15.12.2023 Revised: 28.01.2024 Accepted: 06.02.2024

Analysis of Vibration and Acoustic Sound Radiation of a Rotationally Symmetrical Plate

Kleandro Koka[1*], Klodian Dhoska[2], Andrea Bylykbashi[3]

[1] Institute of Mechanics and Mechatronics, Faculty of Mechanical and Industrial Engineering, Vienna University of Technology, Austria
[2] Faculty of Engineering, Canadian Institute of Technology, Albania
[3] World Academy of Tirana, Albania
*kleandro.koka@tuwien.ac.at

Abstract

The importance of studying the vibration and acoustic radiation of symmetrical plates lies in its widespread applications across various engineering disciplines. Symmetrical plates are fundamental structural components found in aerospace, automotive, marine, and civil engineering systems. This study is focused on vibration behaviour and acoustic sound radiation of a rotationally symmetrical plate. Therefore, analysing the vibration behaviour of a rotationally symmetrical plate can be helpful to optimize the mechanical and acoustic properties of such structures. Sweep operation, Lissajous curve and stochastic excitation methods have been used to determine the natural frequencies. The acoustic radiation is measured at various frequencies and distances from the plate using a calibrated microphone.

Keywords: *Vibration, acoustic, natural frequencies, symmetrical plates.*

INTRODUCTION

Symmetrical plates are fundamental structural components found in various engineering disciplines such as aerospace, automotive, marine, and civil engineering systems. The analysis of vibration and acoustic sound radiation in rotationally symmetrical plates is a crucial study in understanding the dynamic behavior and emission characteristics of such structures. Rotationally symmetrical plates, due to their geometric features, exhibit unique vibrational modes and acoustic radiation patterns, making them intriguing subjects for investigation [1-4].

In aerospace engineering, for instance, symmetrical plates form essential components of aircraft wings and fuselage. Knowledge of their vibrational characteristics is vital for designing lightweight yet structurally sound components, while understanding acoustic radiation helps in reducing the overall noise generated during flight. Similarly, in automotive engineering, symmetrical plates are integral parts of vehicle bodies [5, 6]. Analyzing their vibration patterns is essential for improving ride comfort, stability, and overall vehicle performance. Additionally, controlling acoustic radiation is crucial to enhance passenger comfort and meet regulatory noise standards. In marine engineering, symmetrical plates are found in ship structures. Understanding their vibrational behavior is essential for ensuring structural integrity and safety, while controlling acoustic radiation aids in reducing underwater noise pollution, benefiting marine ecosystems. In civil engineering, symmetrical plates are used in various structures, such as bridges and buildings [7-9]. Analyzing their vibrations helps in designing structures that can withstand dynamic loads, wind, and seismic forces. Controlling acoustic radiation is important for minimizing the impact of noise on nearby environments. Importance of the study of vibration and acoustic radiation of symmetrical plates is indispensable for optimizing structural design, ensuring safety and

durability, and meeting environmental and regulatory standards across a range of engineering applications [10-12].

This article presents an analysis of the vibration behaviour of a rotationally symmetrical plate that can be helpful to optimize the mechanical and acoustic properties of such structures. Sweep operation, Lissajous curve and stochastic excitation methods have been used to determine the natural frequencies. The acoustic radiation is measured for different frequencies and distances from the plate and compared with theoretical values.

MEASUREMENT SETUP

The experiments are carried out in a soundproof studio box that serves as an acoustic laboratory. The measurement object is a flat, rotationally symmetrical acrylic glass plate. There is an electrodynamic vibration exciter under this plate, see Figure 1.

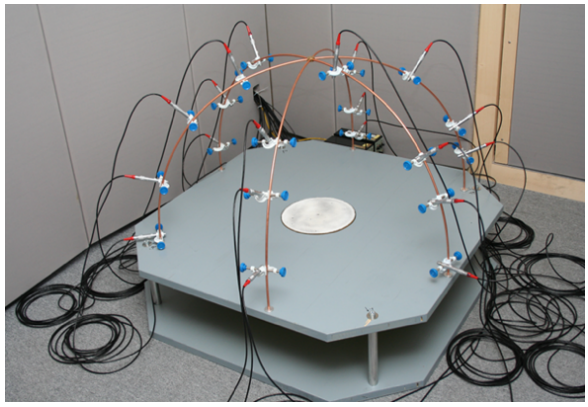

Figure 1. Experimental setup view of rotationally symmetrical acrylic glass plate

The impedance measuring head, which is connected to the charge amplifiers, lies between the plate and the electrodynamic vibration exciter. There are also 20 microphones evenly spaced across the panel on three guides that form a hemispherical shape. All microphones, charge amplifiers and electrodynamic vibration exciters are wired and laid outside the studio box. Outside the studio box is the audio interface, oscilloscope, the Peripheral module (PXI) system which has been installed with field programmable gate arrays (FPGA) module, and the CA-1000 module, see Figure 2.

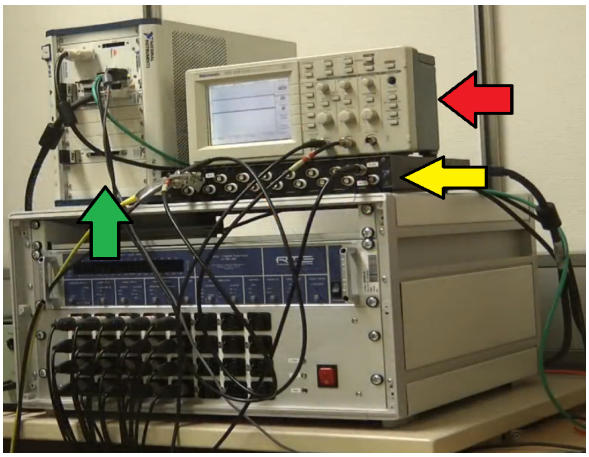

Figure 2. PXI system (green), CA-1000 module (yellow), oscilloscope (red)

The PXI system regulates and acquires the analogue signals from the charge amplifiers, which are then transferred to the CA-1000 module and converted into digital signals. The PXI system also serves as an output for the vibration exciter's manipulated variable, which was previously amplified by a power amplifier. Table 1 depict the plate measurement parameters.

Table 1. Plate measurement parameters

Parameter	Values	Units
Plate radius (a)	0,1175	m
Plate thickness (h)	$4{,}7 \cdot 10^{-3}$	m
Plate volume (V)	$0{,}8674 \cdot 10^{-3}$	m^3
Density (ρ)	$1{,}18 \cdot 10^{3}$	kg/m^3
Dimensions (m)	1,0236	kg
Youngs Modulus (E)	$4{,}3 \cdot 10^{9}$	Pa
Poisson's ratio (v)	0,33	–

The calculation of the natural frequencies is sufficient to operate an oscillatory system outside of these natural frequencies and thus avoid resonance effects. The boundary conditions for this plate are as follows:

- No moment at the radius
- No lateral force at the radius

Based on it, the natural frequencies w_S have been calculated through equation 1.

$$w_S = \frac{\lambda_S^2}{a^2} \cdot \sqrt{\frac{D}{\mu}} \tag{1}$$

Where D is bending stiffens, μ is mass per aria and λ_s^2 is the eigen parameter. The bending stiffness and mas per area has been calculated respectively by using equations 2 and 3.

$$D = \frac{Eh^3}{12(1-v^2)} \tag{2}$$

and

$$\mu = \rho \cdot h \tag{3}$$

Furthermore, the individual frequencies f_S has been calculated through equation 4.

$$f_S = \frac{w_S}{2\pi} \tag{4}$$

Sweep Operation

The first of the three ways to determine the natural bending frequencies of the plate is the sweep operation. By harmoniously exciting the plate through constant force over the frequency, the acceleration of the excitation can be determined using the built-in impedance measuring head. The spectrum is carried out at appropriate speed in both positive and negative directions. The experiment had a frequency spectrum of 200 Hz to 2000 Hz. The

recordings of the amplitude response were superimposed in the positive and negative directions to determine whether the rate of increase was chosen correctly. If the speed was too high, different peaks would occur at the resonance frequency.

The charge amplifiers have been adjusted till the sensitivities match the structure. The sensitivity of the entire measuring chain E_T results from the following relationship by using equation 5.

$$E_{\mathrm{T}} = \frac{E_S}{E_A} \cdot \frac{E_M}{k_{AG}} \tag{5}$$

Where, E_{s} is sensitivity of the measuring chain, E_{A} is the sensitivity of charge amplifier, E_{M} is sensitivity of the force, k_{AG} is setting of the output size.

Based on our data, the converter sensitivity corresponds to $E_{\mathrm{S}} = 3.27\ \mathrm{pC/ms^{-2}}$ according to the sensitivity of the impedance measuring head. The sensitivity of the entire measuring chain is $10\ \mathrm{mV/ms^{-2}}$ and the sensitivity of the transducer is $E_{\mathrm{A}} = 3.27\ \mathrm{pC/ms^{-2}}$. In addition, it is necessary to select the unit with a low frequency limit of 2 Hz and a high frequency limit of 10,000 Hz. The sensitivity of the measuring amplifier is $E_{\mathrm{M}} = 10\ \mathrm{mV}$.

Lissajous Curve

A Lissajous curves has been used to provide a parametric display of two waves overlaid on the same graph. It has been created when two harmonic oscillations are superimposed at right angles to each other and have different frequencies. In Lissajous mode, the x and y inputs of the oscilloscope are connected to two signals, resulting in a Lissajous curve on the screen. The ratio of the frequencies and the phase shift of the signals determine the shape of the figure. An ellipse or circle is created when the frequencies are the same. A closed figure with multiple loops is created when the frequencies have a rational relationship. A non-periodic figure fills the entire image when the frequency ratio is irrational. The angle between the main axes of the figure and the coordinate axes indicates the phase shift.

The velocity signal is now required on the X-axis and the force signal on the Y-axis of the oscilloscope. The charge amplifier of the force remains unchanged, but the acceleration amplifier needs to be changed a lot. However, we already measure the acceleration, but we want to display the velocities in our oscilloscope. That's why we have to change the units to m/s and the lower frequency limit of and also the gain to 100. When making this change, care must be taken to ensure that we have the integration constant. The sensitivity of the entire measuring chain corresponds to the value $10\ \frac{V}{m/s}$ which is calculated by using above equation 5 for 10 Hz and $k_{AG} = 0.01$.

Furthermore, Channel 1 of the oscilloscope is therefore at the input of the velocity signal of the CA-1000 module and Channel 2 is at the input of the force signal. It has been represented the speed signal on the X-axis and the force signal on the Y-axis.

Stochastic Excitation

The natural frequency is determined by random excitation with stochastic excitation, a so-called random signal. In contrast to previous attempts to regulate the excitation force to a target value, this is now no longer necessary. This method transmits the signals generated by the impedance measuring head via a charge amplifier to the signal analyser, which determines the natural frequencies by calculating the transfer function.

The charge amplifier from the force signal must be set back to the sweep settings (acceleration signal with $k_{AG} = 1$ and $E_T = 10\frac{mV}{ms^{-2}}$. The soundproof foam boxes will also be

removed. The signals that have been measured are fed to the signal analyser. It is important that the CA-1000 module is correctly connected from the force signal to Channel 1 and from the acceleration signal to Channel 2. The CA-1000 module disconnects the oscilloscope. LabVIEW has been used to control the noise excitation of the EDSE with an “averaging mode” of root mean square (RMS), a linear “weighing mode” and a “number of averages” of 16. After the signal analyser is switched on, the corresponding transfer function is loaded onto the diskette. The transfer function $G(\omega)$ is calculated through equation 6:

$$G(\omega) = \frac{S_{aF}(\omega)}{S_{FF}(\omega)} \tag{6}$$

Where $S_{aF}(\omega)$ is cross power density of force and acceleration, and $S_{FF}(\omega)$ is power density.

The use of the transfer function enables the convenient calculation of natural frequencies due to the small deviations.

Acoustic Measurements

In acoustic measurement, a pressure velocity (PV) probe is used to accurately measure the radiated power of the plate excited at natural frequency. Due to the absence of a dedicated probe, the measurement is approximated using the envelope method with microphones arranged in a hemispherical shape. The sound pressure level measured by the microphones is converted into a time-averaged sound pressure level. In contrast to previous attempts, the charge amplifier is not used for acceleration. However, the charge amplifier settings for the force remain unchanged. It is also necessary that the input level of the audio interface is +19 dB because this corresponds to the input gain of the analogue-to-digital converter.

Before we can carry out the test and measurement, we need to calibrate all 20 microphones. To achieve this, a pistonphone, a Sound Calibrator Type 4231 was used as can be seen in Figure 3. An adapter connects the microphone to the pistonphone's sound pressure chamber. The movement of the piston in the sound pressure chamber of the pistonphone creates a sinusoidal alternating pressure. At a frequency of 1kHz, the precision sound source produces a constant sound level of 1 Pa. Since the sensitivity of the microphones ideally remains constant, calibration at one frequency is sufficient. It is now possible to calibrate the microphone via the LabView interface using the corresponding button. The "number 20" microphone has been selected in the centre of rotationally symmetrical acrylic glass plate as the best position with a sensitivity of 5.723 V/Pa. The pistonphone is now removed, and the microphone is returned to its proper place in the hemispherical construction.$E_{20,L}$.

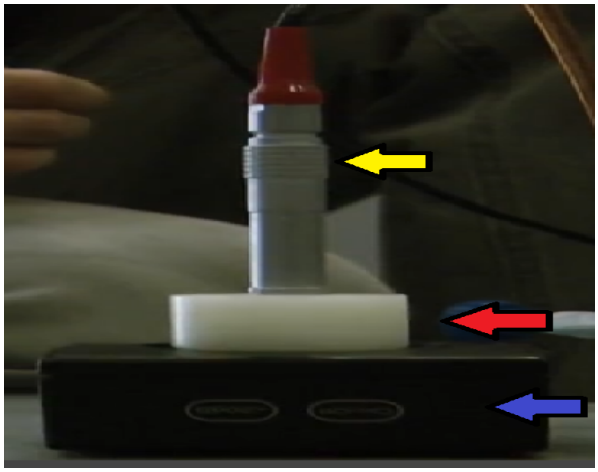

Figure 3. Pistonphone (blue), adapter (red), microphone (yellow)

Only a portion of the data captured by the microphone is shown here for demonstration. It has been calculated the sensitivity by dividing the sound pressure used for calibration by the RMS value of the sinusoidal oscillation, see equation 7 and 8 [13-15].

$$x_{eff} = \sqrt{\frac{1}{N}\sum_{i=1}^{N} x_i^2} \tag{7}$$

and

$$E_T = \frac{x_{eff}}{p_{ref}} \tag{8}$$

Where x_{eff} is RMS value, x_i is individual measurement values of the microphones, N is number of measurement data and p_{erf} is the reference pressure with 1 Pa.

Before we can carry out the experiment, we have attached the foam boxes to the electrodynamic sound generator to acoustically isolate it. This prevents acoustic excitation signals from entering the recording.

Afterward, the LabVIEW user interface is used to start the test. The duration of the test or recording time of the microphones is 3 seconds and the sampling frequency is 44100 Hz. This leads to a resolution of the frequency of 0,333 Hz. Now we select the mode for measuring the sound intensity and the first natural frequency of 305 Hz. The electrodynamic sound generator and the microphone recording are activated, and the collected measurement data is saved. The second natural frequency of 1212 Hz and the intermediate frequency of 490 Hz are treated with the same procedure. The measurement at 490 Hz serves as a comparison. Table 2 depict the parameters of the sound pressure and sound power level.

Table 2. Parameters for the calculation of the sound pressure and sound power level

Parameters	Values	Units
Entire sound area (A_m=A_{HK})	1.571	m^2
Area per microphone (A_i)	0.07855	m^2
Reference surface (A_0)	1	m^2
Reference pressure (p_0)	$20 \cdot 10^{-6}$	Pa
Reference power (P_0)	10^{-12}	W
Characteristic acoustic impedance at standard conditions ($Z_{a,k}$)	411.5	Ns/m^3

Furthermore, we also use the correction factor C_1 through equation 9.

$$C_1 = 10 \cdot log\left(\frac{p_0^2 \cdot A_0}{\rho_0 \cdot c_0 \cdot P_0}\right) \tag{9}$$

Afterward by using equation 10 we have calculated the time-averaged sound pressure level L_{pa}.

$$L_{pa} = 10log\left(\frac{\frac{1}{N}\sum_{i=1}^{N} p_{a,i}^2}{p_0^2}\right) = 20log\left(\frac{\sqrt{\frac{1}{N}\sum_{i=1}^{N} p_{a,i}^2}}{p_0}\right) \tag{10}$$

The calculation of inhomogeneity measure V_i is calculated through equation 11.

$$V_i = \sqrt{\frac{1}{N_M - 1}\sum_{i=1}^{N_M}\left(L_{pa,i} - L_{pa,av}\right)^2} \tag{11}$$

Then we calculate the time-average measuring surface sound pressure level $\underline{L_{pa}}$, se equation 12.

$$\underline{L_{pa}} = 10log\left(\frac{1}{A_m}\sum_{i=1}^{N_M} A_i \cdot 10^{0,1L_{pa,i}}\right) \tag{12}$$

Finally, we determine the average sound power level $\underline{L_{Pav}}$, see equation 13.

$$\underline{L_{Pav}} = \underline{L_{pa}} + 10log\left(\frac{A_{HK}}{A_0}\right) + C_1 + C_2 + C_3 \tag{13}$$

MESUREMENT RESULTS

In this section we will briefly describe the measurement and numerical results for vibration and acoustic sound radiation of our rotationally symmetrical plate.

Table 3 and 4 will show the numerical results of natural and individual frequencies in vibration measurements.

Table 3. Numerical results of natural frequencies

$w_1 = 1805.25\ s^{-1}$	$w_2 = 7661.01\ s^{-1}$	$w_3 = 17448.42\ s^{-1}$	$w_4 = 31200.50\ s^{-1}$

Table 4. Numerical results of individual frequencies

$f_1 = 287.31$ Hz	$f_2 = 1219.29$ Hz	$f_3 = 2777.00$ Hz	$f_4 = 4965.71\ Hz$

Sweep Operation Results. The following results for sweep operation are shown in Table 5 and Figure 4.

Table 5. Sweep operation results

	Negative Sweep		**Positive Sweep**	
Natural Frequencies	1	2	1	2
Frequencies (Hz)	296.50	1210.74	305.55	1234.64
Amplitude (mV)	300.90	743.10	292.97	730.29
Amplitude acceleration (m/s^2)	30.09	74.310	29.3	73.029

In the beginning of our measurement results we have performed a sweep experiment with a frequency of 35 Hz. Afterward we can see how the peaks behave, we plotted both the positive and negative sweep directions in MATLAB. By superposing both graphs, we could notice that the peaks superimpose very well on each other, which means to us that we have chosen the slew rate correctly. The peaks in the positive sweep direction were approximately 305.55 Hz and 1234.64 Hz and in the negative sweep direction 296.5 Hz and 1210.74 Hz, which were not very far from estimated values, which is what we also used Graphs can

confirm. By comparing with the analytical values, there is a deviation of 3.80% for positive sweep and 1.25% for negative sweep.

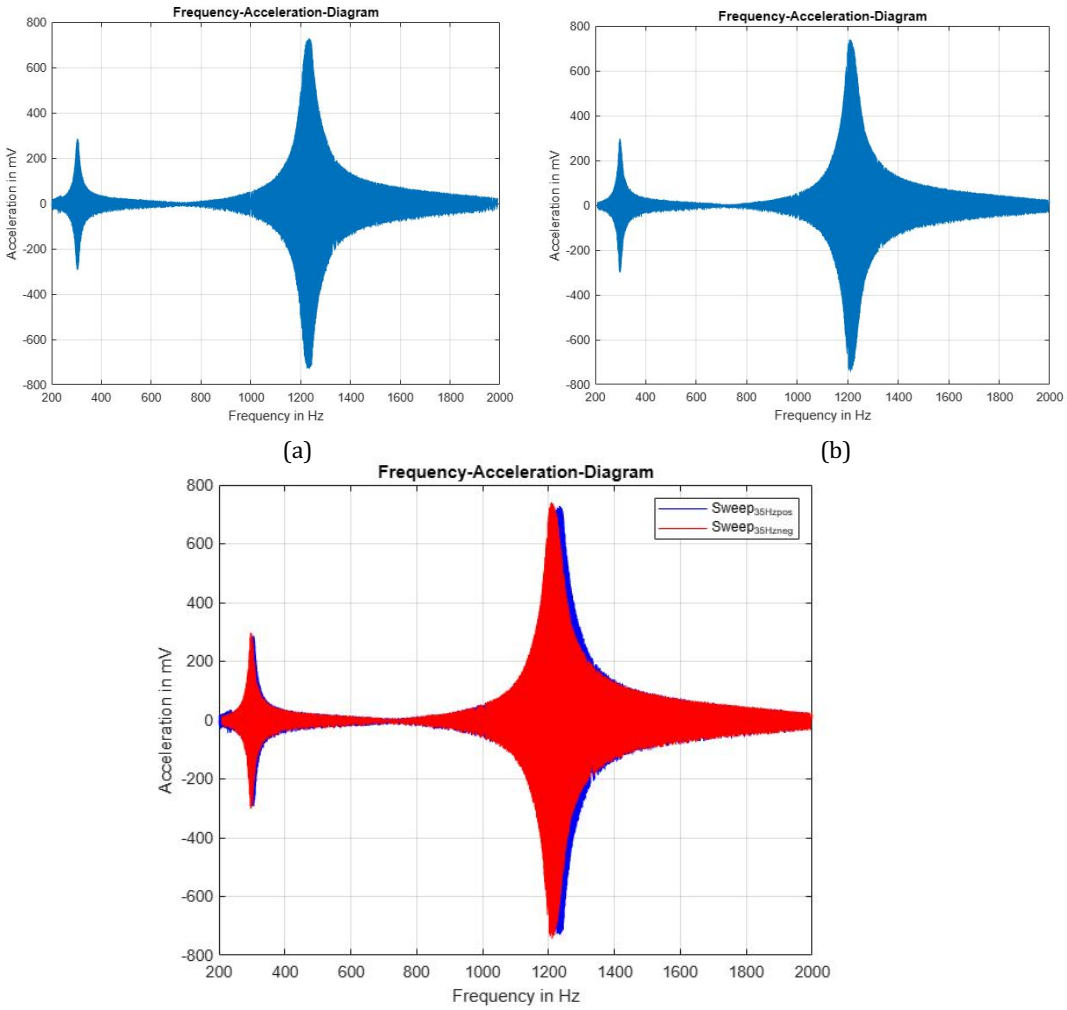

Figure 4. Frequency-Acceleration-Diagram, (a) sweep operation positive (b) sweep operation negative (c) overlay

Lissajous Results. The desired values were determined using the natural frequencies 305 Hz and 1212 Hz . Taking the sensitivity into account, we obtain the speeds and forces for both frequencies as can be seen in Table 6.

Table 6. Speeds and forces for both frequencies

Natural Frequency (Hz)	Speed (m/s)	Speed (m/s)	Power (N)	Power (N)
	$V_{max(,pos)}$	$V_{max(,neg)}$	$F_{max(,pos)}$	$F_{max(,neg)}$
$f_1 = 305$	0.1815	0.17486	0.108032	0.1215
$f_2 = 1212$	0.06012	0.05157	0.102844	0.1062

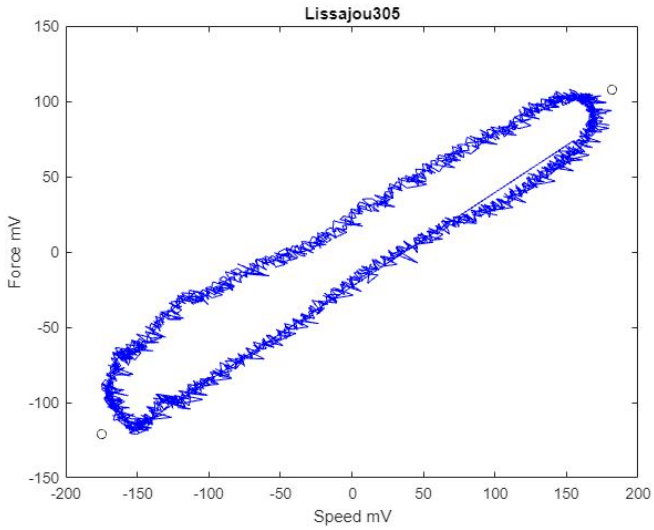

(a)

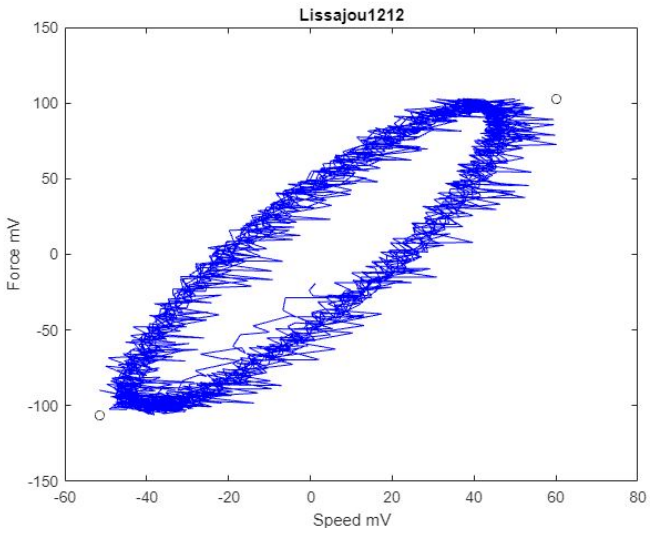

(b)

Figure 5. Speed and force behaviour in Lissajous results

The second experiment was Lissajous with a frequency of 305 Hz. We can clearly see here that the curve approaches a straight line. But at the second frequency of 1212 Hz, an elliptical shape has appeared. We decided to believe the representations on the oscilloscope rather than those in LabVIEW because such deviations are caused by the PXI system, which makes small errors in the control that distort the curves in LabVIEW. With the analytical calculation we find a difference of 2.78%.

Stochastic Excitation Results. The natural frequencies results in stochastic excitation are shown in Table 7 and Figure 6

Table 7. Results of natural frequencies in stochastic excitation

$f_1 = 320$ Hz	$f_2 = 1220$ Hz	$f_3 = 2860$ Hz	$f_4 = 5380$ Hz

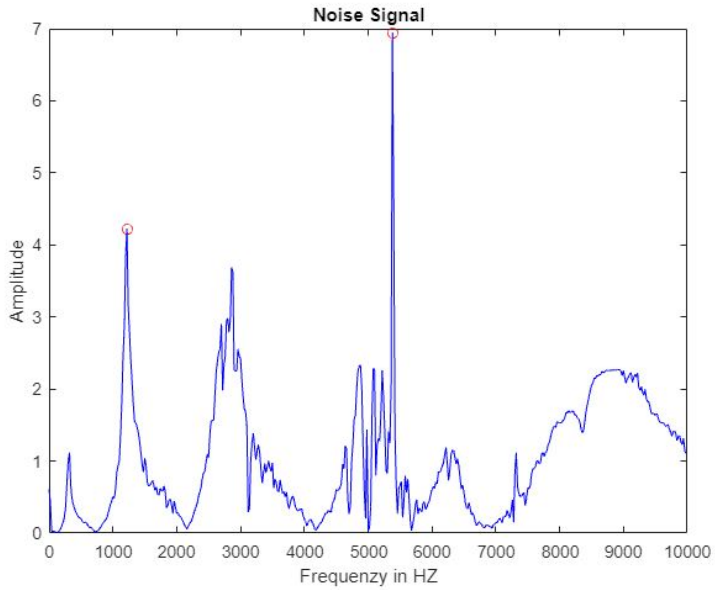

Figure 6. Noise signal

With stochastic excitation, the natural frequencies were determined using a frequency analyser, which displayed different peaks in the frequency spectrum. The first 4 peaks were around $f_1 = 320$ Hz , $f_2 = 1220$ Hz , $f_3 = 2860$ Hz $f_4 = 5380$ Hz. These values correspond to the resonance frequencies at different excitation strengths, whereby we took peaks into account for the first two peaks because the other methods had a limited frequency spectrum and only allowed measurements up to approx. in sweep mode. With stochastic excitation, the first 2 frequencies deviated the most from the analytical calculation by almost 5.72 %.

Acoustic Results. The calibration results of the 20 microphones for the frequencies 305 Hz, 490 Hz and 1212 HZ are shown in the Table 8.

In this experiment, we also measured the sound power level at different frequencies. We used 20 microphones arranged around the record. Before measuring, we calibrated the Microphone 20 to correct possible deviations. This would have a deviation of 4.14% from the specified sensitivity. If we had not calibrated the microphone 20, we would have received incorrect measurement data that could distort the sound power level. This would have led to incorrect conclusions about the dependence of the sound power level on frequency. Therefore, calibrating microphone 20 was an important step in this experiment. The results showed that the sound power level was different at the three frequencies. At 305 Hz the average sound power level was approximately $L_{Pa} = 74{,}06$ dB and at 1212 Hz it was $L_{Pa} = 84{,}00$ dB . These values show that the sound power level increases with frequency because higher frequencies transmit more energy, which is to be expected.

The surprising aspect was that the measurement at 490 Hz correspond to $L_{Pa} = 68{,}54$ dB which was not what we expected. We obtained a lower average value in comparison of 305 Hz despite having a higher natural frequency. It is possible that this result is due to an error in the measurement. The calibration should be checked several times for future measurements.

Table 8. Microphones calibration

	Measurement (305 Hz)	**Measurement (490 Hz)**	**Measurement (1212 Hz)**
Microphones	Time-average sound pressure level in dB	Time-average sound pressure level in dB	Time-average sound pressure level in dB
1	72.86225591	68.07102774	76.18691223
2	69.50838214	67.60761303	78.91585197
3	74.05502855	67.84920279	82.18711863
4	73.83499854	67.50484329	83.98657503
5	72.03885071	67.22776287	81.70365161
6	71.72099950	67.33314337	74.86444099
7	74.48254752	67.52012724	79.91091564
8	73.73272771	67.62497446	77.66457511
9	68.43484829	66.84994896	81.66334957
10	70.82160613	65.86286118	75.41943301
11	73.17469639	65.49566606	79.29042637
12	71.58205581	67.00789389	83.71935788
13	67.99117279	66.08735917	80.89723441
14	75.05071646	67.22803585	80.98503242
15	72.08182721	64.22661616	82.48855088
16	69.65751137	65.79193302	79.95517441
17	69.64719798	65.08536091	84.84975456
18	73.16909301	64.46489287	85.07696875
19	72.63375012	66.88518027	83.83540456
20	**68.21596911**	**65.65138271**	**87.19963992**
Mean value	72.0603	66.9465	81.3242
Inhomogeneity measure	0.0265	0.0145	0.0401
Average sound power level	74.0563	68.5438	84.0017

Afterward, the best measurement data results for sound radiation and position has been selected from microphone 20 which correspond to bold value. Based on it, the evaluation of measurement data is depicted in Figure 7 and Table 9.

Table 9. Evaluation of the signal measurement data from the microphone 20

$x_{average}$	**0.392 V**
x_{max}	9.495 V
x_{min}	8.968 V
$E_{20,B} = x_{eff}$	5.878 V
$E_{20,L}$	5.723 V/Pa

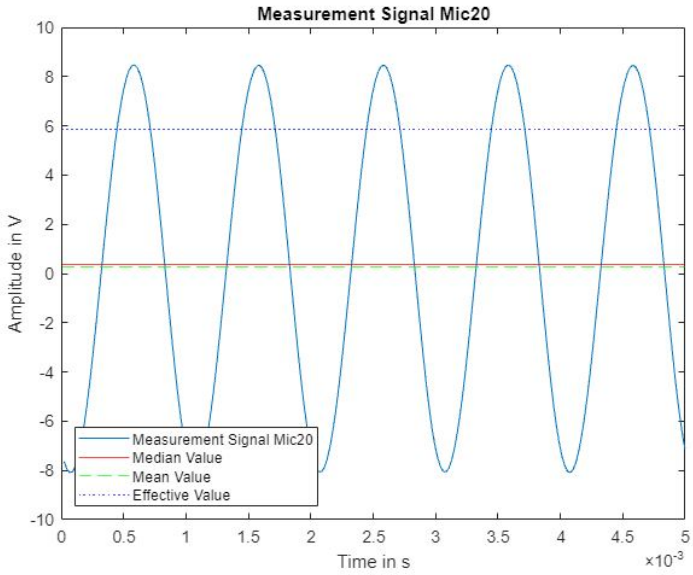

Figure 7. Signal measurement for Microphone 20

Table 10 summarized the results of the natural frequencies for sweep operation, Lissajous and stochastic excitation by accompanied with analytical values.

Table 10. Summarized results of the natural frequencies

Natural frequencies (Hz)	Positive sweep	Negative sweep	Lissajous	Stochastic excitation	Analytical values
1	305.55	296.5	305	320	287,31
2	1234.64	1210.74	1212	1220	1219,29

Table 11 depict the deviations of the natural frequencies measurement results compared to the analytical calculations.

Table 11. Deviations of the natural frequencies measurement results compared to analytical calculations

	Positive Sweep	Negative Sweep	Lissajous	Stochastic excitation
Deviation (%)	3.8	1.25	2.78	5.72

SUMMARY AND CONCLUSIONS

In this paper we have analyzed the vibration and acoustic radiation of the rotational symmetrical plate. It has been determined the natural bending frequencies through sweep operation, Lissajous and stochastic excitation. The acoustic radiation is measured for different frequencies and distances from the plate. The main conclusions are summarized as follows:

- The peaks in the positive sweep direction were approximately 305.55 Hz and 1234.64 Hz and in the negative sweep direction 296.5 Hz and 1210.74 Hz. The deviation of 3.80% correspond for positive sweep and 1.25% for negative sweep.

- In Lissoujus results at frequency 305 HZ it has been seen the curve that approaches a straight line and for the frequency of 1212 Hz is appeared an elliptical shape. The deviation corresponds to the value 2.78%.
- In stochastic excitation results the first 4 peaks were displayed in the frequency spectrum and corresponds to the values $f_1 = 320$ Hz , $f_2 = 1220$ Hz , $f_3 = 2860$ Hz $f_4 = 5380$ Hz. the first 2 frequencies deviated the most from the analytical calculation by almost 5.72 %.
- The sound power level was different at the three frequencies. At 305 Hz the average sound power level was approximately $L_{Pa} = 74{,}06$ dB and at 1212 Hz it was $L_{Pa} = 84{,}00$ dB . The sound power level increases with frequency due to higher frequencies transmit more energy, which is to be expected.
- Due to an error in our measurements it has been detected a surprising aspect for the measurement value at 490 Hz which correspond to $L_{Pa} = 68{,}54$ dB. We have obtained a lower average value in comparison to 305 Hz despite having a higher natural frequency.
- The "number 20" microphone has been selected in the centre of rotationally symmetrical acrylic glass plate as the best position with a sensitivity of 5.723 V/Pa.

CONFLICT OF INTERESTS

The authors would like to confirm that there is no conflict of interests associated with this publication and there is no financial fund for this work that can affect the research outcomes.

REFERENCES

[1] Dickinson S.M. The flexural vibration of rectangular orthotropic plates subject to in-plane forces. *Journal of Applied Mechanics*, 1971; 38; 699-700.

[2] Sun Y. Vibration and Acoustic Radiation of Stiffened Plates Subjected to In-Plane Forces. *Advances in Civil Engineering*, 2022; 9917664.

[3] Jin G., Ma L., Zhang H., and Wang Q. Vibration Characteristics Analysis of Composite Laminated Annular/Circular Plate Using High-Order Shear Deformation Theory, *Shock and Vibration*, 2021, 5913860.

[4] Afsharmanesh B., Ghaheri A., and Taheri-Behrooz F. Buckling and vibration of laminated composite circular plate on Winkler-type foundation. *Steel and Composite Structures*, 2014; 17(1); 1-19.

[5] Yang T., Zheng W., Huang Q., and Li S. Sound radiation of functionally graded materials plates in thermal environment. *Composite Structures*, 2016; 144; 165-176.

[6] Pandey A.M., Gopal K.V.N. Transient vibration and sound radiation analysis of simply supported functionally graded sandwich plates. *Composite Structures*, 2022; 290; 115520.

[7] Singh B.N., Hota R.N., Dwivedi S., Jha R., Ranjan V., Řehák K. Analytical Investigation of Sound Radiation from Functionally Graded Thin Plates Based on Elemental Radiator Approach and Physical Neutral Surface. *Appl. Sci.,* 2022, 12, 7707.

[8] Geng Q., Li H., Li Y. Dynamic and acoustic response of a clamped rectangular plate in thermal environments: Experiment and numerical simulation. *J. Acoust. Soc. Am.,* 2014; 135; 2674-2682.

[9] Alshabatat N., Naghshineh K. Minimizing the radiated sound power from vibrating plates by using in-plane functionally graded materials. *Journal of Vibroengineering*, 2021; 23(3); 744-758.

[10] Du Y., Li H., Gong Q., Pang F., Sun L. Dynamic and Sound Radiation Characteristics of Rectangular Thin Plates with General Boundary Conditions. *Curved and Layer. Struct.*, 2019; 6; 117-131.

[11] Liew, K.M., K.Y. Lam, and S.T. Chow, Free vibration analysis of rectangular plates using orthogonal plate function. Computers & Structures, 1990. 34(1): p. 79-85.

[12] Sulejmani A., Koça O., Dhoska K., Gheibi M., Moezzi R. A novel method of jacobian contours to evaluate the influence line in statically determinate structures. *Appl. Mech.*, 2023; 4(4); 1172-1187.

[13] Dhoska K., Lumi D., Sulejmani A., Koça O. Measurement uncertainty for mechanical resistance of manufactured steel bar. *Pollack Periodica*, 2022; 17(2); 104-108.

[14] Dhoska K., Tola S., Pramono A., Vozga I. Evaluation of measurement uncertainty for the determination of the mechanical resistance of the brick samples by using uniaxial compressive strength test. *Int. J. Metrol. Qual. Eng.*, 2018; 9(12); 1-5.

[15] Dhoska K., Hofer H., Rodiek B., López M., Kübarsepp T., Kück S. Improvement of the detection efficiency calibration and homogeneity measurement of Si-SPAD detectors. *Springerplus*, 2016; 5(1); 2065.